Similarity laws of the fiber-matrix interface crack in Fiber-Reinforced Polymer Composites

Luca Di Stasio[a,b], Janis Varna[a], Zoubir Ayadi[b]

[a] *Luleå University of Technology, University Campus, SE-97187 Luleå, Sweden*
[b] *Université de Lorraine, EEIGM, IJL, 6 Rue Bastien Lepage, F-54010 Nancy, France*

Abstract

Keywords: Fiber Reinforced Polymer Composite (FRPC), Debonding, Similarity, Dimensional analysis

---

1. Introduction

One of the most promising developments in Fiber Reinforced Polymer Composites (FRPCs) for advanced structural applications is currently represented by *thin-ply* laminates [1]. Constituted by extremely thin plies, with t_{90° as small as just $\sim 4-5$ fiber diameters, this family of laminates is characterized by its damage tolerance, in particular the capability of delaying to higher strains and even suppressing the onset and propagation of transverse cracks [2]. The recent experimental assessment of transverse cracks suppression in *thin-ply* laminates [3, 4, 5] validates the existence of a *ply-thickness* effect [5] at scales $10x$ smaller than those at which it was originally observed at the end of the 1970's [6].

Onset of transverse cracks coincides at the microscopic level with the formation of fiber/matrix interface cracks [7], or debonds. After the inter-fiber stress [8] and strain concentration [9] causes the matrix to fail at or close to the fiber interface, debonds grow along the fiber arc direction until a maximum or critical size is reached. If the applied load is increased, debonds move into the matrix or "kink" out of the fiber/matrix interface [10, 11]. Coalescence of debonds then occurs, which corresponds macroscopically to through-the-thickness transverse crack propagation [10, 12]. Finally, propagation through the specimen width occurs [10].

Given that *thin-plies*, as previously noted, can reach nowadays thicknesses of just $\sim 4-5$ fiber diameters, the characteristic size of the ply, i.e. the thickness $t_{90^{\circ}}$, is now comparable in magnitude to the characteristic size of debonds, i.e. the fiber diameter $2R_f$, such that $t_{90^{\circ}}/(2R_f) \sim \mathcal{O}(1)$. This has motivated in recent years a renewed interest in debond growth modeling [13, 14, 15, 16]. Since the elastic solution to the interface crack problem implies an oscillating solution at the crack tip [17] in the *open* case (crack faces not in contact), Stress Intensify Factors (SIFs) are not defined and debond growth characterization has focused on the determination of Mode I, Mode II and total Energy Release Rate (ERR). Many authors have reported their results in normalized form [11, 18, 19], by defining a reference ERR G_0. The definition of such reference ERR would be useful to establish similarity laws and thus to allow comparisons between different material systems, scales, loads and microstructural arrangement. However, no agreement can be found in the literature on the very definition of G_0 and expressions vary between authors. Furthermore, no clear derivation of G_0 has been proposed. In this brief contribution, we provide a derivation of G_0 based on arguments of dimensional analysis, material homogenization and fracture mechanics; we then apply the derived expression of reference ERR to the analysis of debond growth in Representative Volume Elements (RVEs) of UD composites and cross-ply laminates.

2. Dimensional analysis

We first recall that the Energy Release Rate G has units of energy E per unit area:

$$[G] = \frac{E}{L^2}, \tag{1}$$

where L stands for unit of length. By algebraic manipulation of Equation 1 we can write the units of ERR as

$$\frac{E}{L^2} = \frac{F \cdot L}{L^2} = \frac{F}{L^2}\frac{L}{L}L, \tag{2}$$

where F stands for unit of force. We recognize that, in Equation 2

$$\frac{F}{L^2} = [\sigma] \qquad \frac{L}{L} = [\varepsilon], \tag{3}$$

where σ and ε are respectively stress and strain. The reference Energy Release Rate is thus dimensionally equivalent to a reference stress σ_{ref} times a reference strain ε_{ref} times a refence length l_{ref} and we can write

$$G_0 \sim \sigma_{ref}\varepsilon_{ref}l_{ref}. \tag{4}$$

3. Linear Elastic Fracture Mechanics (LEFM) considerations

In the case of uniaxial loading, we can assume that: in a stress-controlled experiment, σ_{ref} is equal to the applied stress σ_0 and ε_{ref} to the average strain ε_0 in the Representative Volume Element (RVE); in a strain-controlled experiment, ε_{ref} is equal to the applied strain ε_0 and σ_{ref} to the average stress σ_{av} in the Representative Volume Element (RVE).

Under the assumption of linear elastic material constituents, we have, respectively for a stress- and strain-controlled experiment:

$$\varepsilon_{av} = E_{homo}\sigma_0 \qquad \sigma_{av} = E_{homo}\varepsilon_0, \tag{5}$$

where E_{homo} is a homogenized RVE Young's modulus which measures the RVE elastic response in the presence of different material phases and damage. It is worth to point out here that, as we are interested in studying debond growth in the context of transverse crack onset, RVEs are loaded in the direction transverse to the fibers in the layer where debonds are present. Furthermore, we consider RVEs that are 2-dimensional and under the assumption of plane strain or plane stress conditions. This implies, considering the elastic response of a transversely isotropic material in its plane of transverse isotropy (indeces $2-3$, index 1 corresponds to the axis of rotational symmetry) with no damage, that [20, 21]

$$E_{homo} = \frac{E_2}{1-\nu_{12}\nu_{21}} \qquad E_{homo} = E_2, \tag{6}$$

respectively for plane strain and plane stress, with E_2 the homogenized transverse Young's modulus of the ply and ν_{12}, ν_{21} the major and minor Poisson's ratios. Notice that homogenized elastic properties depend on consittuents' elastic properties and theIn the presence of damage, we can assume the homogenized Young's modulus of the damaged RVE to be a fraction of the undamaged modulus E^0_{homo} (expressed in Eq. 6):

$$E_{homo} = f\left(\Delta\theta\right) E^0_{homo}, \tag{7}$$

where $0 < f\left(\Delta\theta\right) < 1$ is a function of the damage state in the material, in this case represented by the debond half-size $\Delta\theta$ (debond size is $2\Delta\theta$). By substituting Eq. 5, Eq. 6 and Eq. 7 in Eq. 4, we have

$$G_0 \sim f\left(\Delta\theta\right) \frac{E_2}{1-\nu_{12}\nu_{21}} \varepsilon_0^2 l_{ref} \quad G_0 \sim f\left(\Delta\theta\right) E_2 \varepsilon_0^2 l_{ref}, \tag{8}$$

respectively for plane strain and plane stress conditions under applied strain ε_0, and

$$G_0 \sim f\left(\Delta\theta\right) \frac{1-\nu_{12}\nu_{21}}{E_2} \sigma_0^2 l_{ref} \quad G_0 \sim f\left(\Delta\theta\right) \frac{\sigma_0^2}{E_2} l_{ref}, \tag{9}$$

respectively for plane strain and plane stress conditions under applied strain σ_0. Notice that, incidentally: the plane strain expression in Eq. 9 is the same as the ERR expression used for *in-situ* strenght modeling in [22] and derived in [23] by considering the fiber-reinforced polymer as a 3-phase composite with one phase constituted by sharp voids (cracks)[1]; the plane stress expression in Eq. 9 is the same as the Mode I ERR in [24], derived from the definition of ERR and problem geometry.

In accord with the classic Linear Elastic Fracture Mechanics (LEFM), the Energy Release Rate is directly proportional to the crack size a [25]. Given that $a = R_f 2\Delta\theta$ for debonds, where R_f is the fiber radius, it is reasonable to assume R_f as the reference length:

$$l_{ref} = R_f. \tag{10}$$

The reference Energy Release Rate thus becomes

$$G_0 \sim f(\Delta\theta) \frac{E_2}{1-\nu_{12}\nu_{21}} \varepsilon_0^2 R_f \quad G_0 \sim f(\Delta\theta) E_2 \varepsilon_0^2 R_f, \tag{11}$$

respectively for plane strain and plane stress conditions under applied strain ε_0, and

$$G_0 \sim f(\Delta\theta) \frac{1-\nu_{12}\nu_{21}}{E_2} \sigma_0^2 R_f \quad G_0 \sim f(\Delta\theta) \frac{\sigma_0^2}{E_2} R_f, \tag{12}$$

respectively for plane strain and plane stress conditions under applied strain σ_0.

4. Similarity and geometry correction factor

In agreement with the classic Fracture Mechanics (FM) treatment [25], we can recognize in the function $f(\Delta\theta)$ of Eq. 11 and Eq. 12 the geometry correction factor ($f(a)$ or Y) that establishes the relation of similarity [26]

$$K = f(a)\,\sigma\sqrt{a} \quad \text{or} \quad G = f^2(a)\,\frac{\sigma^2}{E} a \tag{13}$$

[1] Often expressed as $\Lambda_{22}^0 = 2\left(\frac{1}{E_2} - \frac{\nu_{12}^2}{E_1}\right)$, which can be shown to be equivalent to $\Lambda_{22}^0 = 2\frac{1-\nu_{12}\nu_{21}}{E_2}$ by recalling that $\nu_{21} = \frac{E_2}{E_1}\nu_{12}$.

between the Stress Intensity Factor (SIF) K and Energy Release Rate (ERR) G of a generic configuration of structural and crack geometry and the solution for a Center Crack (CC) in an infinite plate

$$K_{CC} = \sigma\sqrt{a} \quad \text{or} \quad G_{CC} = \frac{\sigma^2}{E}a, \tag{14}$$

where the crack size is $2a$. It thus seems reasonable to look for a functional form of $f(\Delta\theta)$ in Eq. 11 and Eq. 12 among known analytical solutions of SIFs and ERRs and such that a physically-meaningful similarity between the two configurations could be established.

- **Straight central crack in an infinite isotropic plate under far-field transverse tension [25].**

  $$f_I(\Delta\theta) = \sin(\Delta\theta) \qquad f_{II}(\Delta\theta) = 0 \tag{15}$$

  It is the simplest choice, based on considering the debond chord $2R_f \sin\Delta\theta$ as its representative size. However, as apparent in Eq. 15, there is no Mode II geometry correction factor available (a straight crack in transverse tension propagates only in Mode I) and it is thus not suited to establish a relation of similarity with debond ERR, which is Mode II dominated for large $\Delta\theta$.

- **Inclined central crack in an infinite isotropic plate under far-field tension [25].**

  $$\begin{aligned} f_I(\Delta\theta) &= \sin(\Delta\theta)\sin^4\left(\frac{\pi}{2} - \Delta\theta\right) \\ f_{II}(\Delta\theta) &= \sin(\Delta\theta)\sin^2\left(\frac{\pi}{2} - \Delta\theta\right)\cos^2\left(\frac{\pi}{2} - \Delta\theta\right) \end{aligned} \tag{16}$$

  A first attempt to amend the shortcomings of Eq. 15 is to consider the geometry correction factor of the inclined crack subjected to transverse load. However, $f_{II}(90°) = 0$ in Eq. 16, which makes also this choice not a good choice to establish a similarity relation with debond ERR (Mode II ERR is well-defined and different from 0 at $\Delta\theta = 90°$ for debonds).

- **Circular crack in an infinite isotropic plate under far-field tension transverse to crack's chord [27].**

$$
\begin{aligned}
f_I\left(\Delta\theta\right) &= \frac{G_I}{\sigma_{ref}\varepsilon_{ref}R} = \frac{1}{2}\sin\left(\Delta\theta\right)\times\\
&\times\left(\frac{1-\sin^2\left(\frac{\Delta\theta}{2}\right)\cos^2\left(\frac{\Delta\theta}{2}\right)}{1+\sin^2\left(\frac{\Delta\theta}{2}\right)}\cos\left(\frac{\Delta\theta}{2}\right)+\cos\left(\frac{3}{2}\Delta\theta\right)\right)^2\\
f_{II}\left(\Delta\theta\right) &= \frac{G_{II}}{\sigma_{ref}\varepsilon_{ref}R} = \frac{1}{2}\sin\left(\Delta\theta\right)\times\\
&\times\left(\frac{1-\sin^2\left(\frac{\Delta\theta}{2}\right)\cos^2\left(\frac{\Delta\theta}{2}\right)}{1+\sin^2\left(\frac{\Delta\theta}{2}\right)}\sin\left(\frac{\Delta\theta}{2}\right)+\sin\left(\frac{3}{2}\Delta\theta\right)\right)^2
\end{aligned}
\tag{17}
$$

The geometry correction factors of Eq. 17 (shown in Fig. 1) present a solution to the issues characterising Eq. 15 and Eq. 16: Mode II is defined and both modes are defined and continuous for $\Delta\theta = 0° - 180°$. By evaluating the elastic properties E_2, ν_{12} and ν_{21} at the value of V_f of the composite under consideration, and substituting Eq. 17 in Eq. 12 and Eq. 11, we obtain the following expressions of reference ERR:

1. Mode I G_{I0} and Mode II G_{II0} ERR of a circular crack of size $a = 2\Delta\theta$ in an infinite isotropic medium

$$
\begin{aligned}
G_{I0} &= f_I\left(\Delta\theta\right)\frac{E_2\left(V_f\right)}{1-\nu_{12}\left(V_f\right)\nu_{21}\left(V_f\right)}\varepsilon_0^2 R_f\\
G_{II0} &= f_{II}\left(\Delta\theta\right)\frac{E_2}{1-\nu_{12}\nu_{21}}\varepsilon_0^2 R_f
\end{aligned}
\tag{18}
$$

2.
$$
G_{I0} = f_I\left(\Delta\theta\right)\frac{\sigma_0^2}{E_2}R_f \quad G_{II0} = f_{II}\left(\Delta\theta\right)\frac{\sigma_0^2}{E_2}R_f \tag{19}
$$

3.
$$
G_{I0} = f_I\left(\Delta\theta\right)\frac{1-\nu_{12}\nu_{21}}{E_2}\sigma_0^2 R_f \quad G_{II0} = f_{II}\left(\Delta\theta\right)\frac{1-\nu_{12}\nu_{21}}{E_2}\sigma_0^2 R_f \tag{20}
$$

4.
$$
G_{I0} = f_I\left(\Delta\theta\right)\frac{\sigma_0^2}{E_2}R_f \quad G_{II0} = f_{II}\left(\Delta\theta\right)\frac{\sigma_0^2}{E_2}R_f \tag{21}
$$

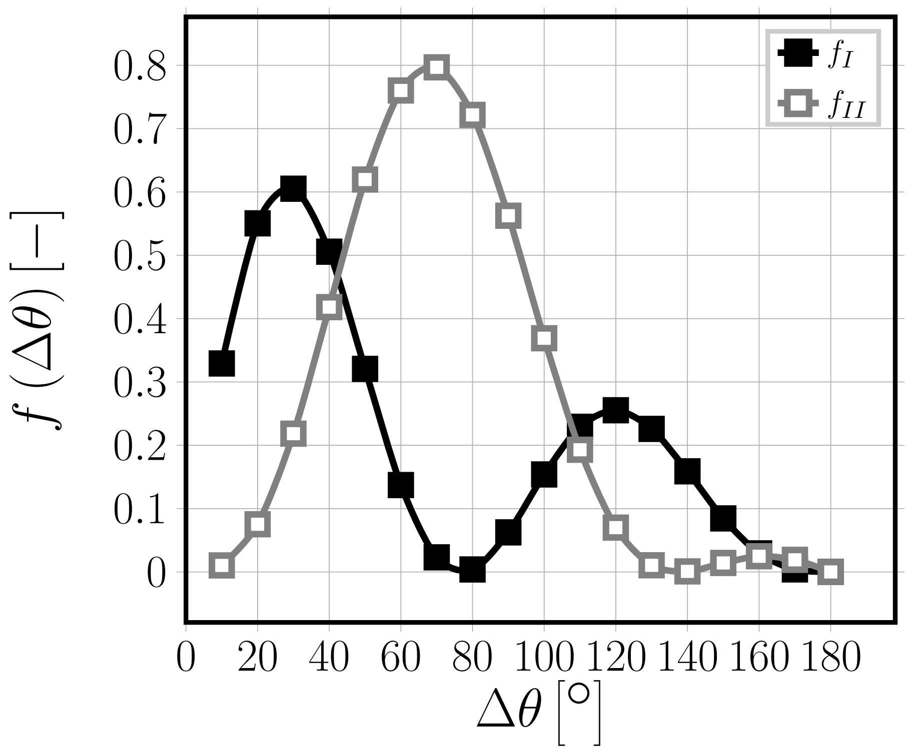

Figure 1: Mode I (f_I) and Mode II (f_{II}) geometry correction functions for a circular crack in infinite isotropic medium. The chord of the crack is normal to the loading direction and the crack size is $a = 2\Delta\theta$.

This configuration establishes also a physically-meaningful relation of similarity, as the ratios $\frac{G_I}{G_{I0}} = g_I(\Delta\theta, V_f)$ $[-]$ and $\frac{G_{II}}{G_{II0}} = g_{II}(\Delta\theta, V_f)$ $[-]$ measure the effect of: the mismatch in elastic properties between phases (in Eq. 17 the medium is isotropic); the finite size of the geometry (in Eq. 17 the medium is infinite); the interaction with neighboring undamaged and partially debonded fibers, a free surface (in UD composites) or the $0°/90°$ interface (in cross-ply laminates).

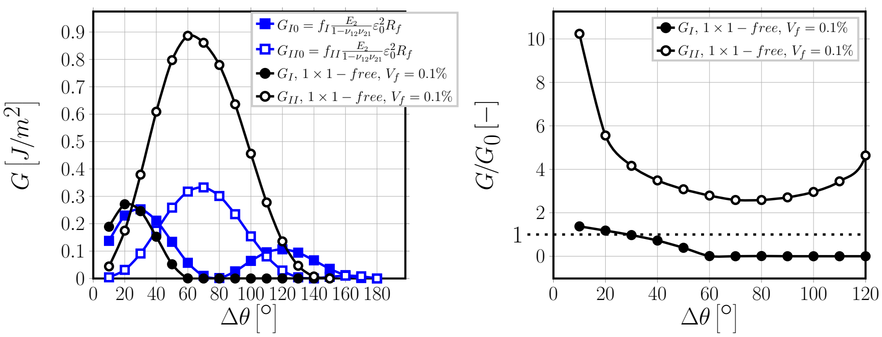

(a) Dimensional ERR.

(b) Normalized ERR.

Figure 2: *Left*: Mode I and Mode II ERR for the circular crack in an infinite isotropic medium (G_{I0} and G_{II0}) and for a single partially debonded fiber in an infinite matrix ($1 \times 1 - free$, $V_f = 0.1\%$). In G_{I0} and G_{II0}, E_2, ν_{12} and ν_{21} are evaluated using the Concentric Cylinders Assembly [28] with Self-Consistent Shear [29] (CCA-SCS) model for $V_f = 0.1\%$. In both cases, a transverse load is applied in the form of transverse strain ε_x of 1%. *Right*: Mode I and Mode II ERR of single partially debonded fiber in an infinite matrix ($1 \times 1 - free$, $V_f = 0.1\%$) normalized by Mode I and Mode II ERR of the circular crack in an infinite isotropic medium (G_{I0} and G_{II0}).

5. Effect of elastic properties mismatch

6. Effect of fiber volume fraction

7. Effect of neighboring fibers

References

[1] A. Kopp, S. Stappert, D. Mattsson, K. Olofsson, E. Marklund, G. Kurth, E. Mooij, E. Roorda, The aurora space launcher concept, CEAS Space Journal 10 (2) (2017) 167–187. `doi:10.1007/s12567-017-0184-2`.

[2] J. Cugnoni, R. Amacher, S. Kohler, J. Brunner, E. Kramer, C. Dransfeld, W. Smith, K. Scobbie, L. Sorensen, J. Botsis, Towards aerospace grade thin-ply composites: Effect of ply thickness, fibre, matrix and interlayer toughening on strength and damage tolerance, Composites Science and Technology 168 (2018) 467–477. `doi:10.1016/j.compscitech.2018.08.037`.

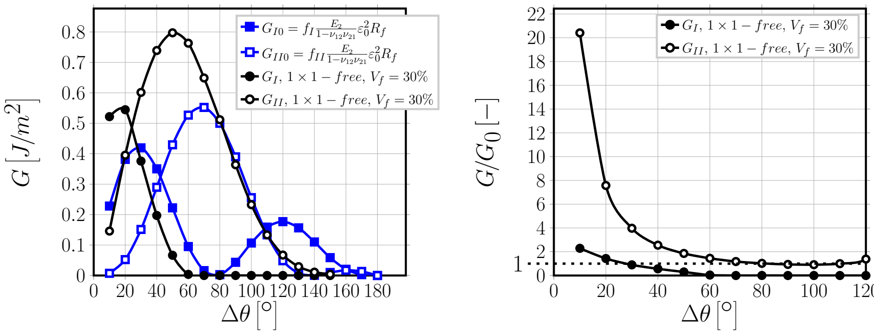

(a) Dimensional ERR.

(b) Normalized ERR.

Figure 3: *Left*: Mode I and Mode II ERR for the circular crack in an infinite isotropic medium (G_{I0} and G_{II0}) and for a single partially debonded fiber in an infinite matrix ($1 \times 1 - free$, $V_f = 30\%$). In G_{I0} and G_{II0}, E_2, ν_{12} and ν_{21} are evaluated using the Concentric Cylinders Assembly [28] with Self-Consistent Shear [29] (CCA-SCS) model for $V_f = 30\%$. In both cases, a transverse load is applied in the form of transverse strain ε_x of 1%. *Right*: Mode I and Mode II ERR of single partially debonded fiber in an infinite matrix ($1 \times 1 - free$, $V_f = 30\%$) normalized by Mode I and Mode II ERR of the circular crack in an infinite isotropic medium (G_{I0} and G_{II0}).

[3] H. Sasayama, K. Kawabe, S. Tomoda, I. Ohsawa, K. Kageyama, N. Ogata, Effect of lamina thickness on first ply failure in multidirectionally laminated composites, in: Proceedings of the 8^{th} Japan SAMPE Symposium, SAMPE, 2003.

[4] H. Saito, H. Takeuchi, I. Kimpara, Experimental evaluation of the damage growth restraining in 90 layer of thin-ply cfrp cross-ply laminates, Advanced Composite Materials 21 (1) (2012) 57–66. `doi:10.1163/156855112X629522`.

[5] R. Amacher, J. Cugnoni, J. Botsis, L. Sorensen, W. Smith, C. Dransfeld, Thin ply composites: Experimental characterization and modeling of size-effects, Composites Science and Technology 101 (2014) 121–132. `doi:10.1016/j.compscitech.2014.06.027`.

[6] J. E. Bailey, P. T. Curtis, A. Parvizi, On the transverse cracking and longi-

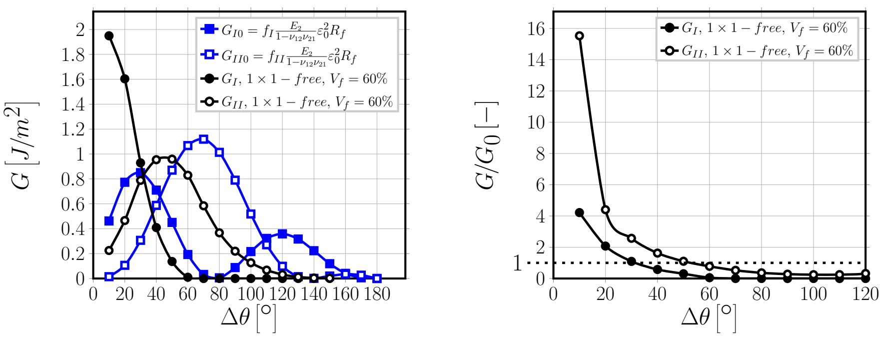

(a) Dimensional ERR.

(b) Normalized ERR.

Figure 4: *Left*: Mode I and Mode II ERR for the circular crack in an infinite isotropic medium (G_{I0} and G_{II0}) and for a single partially debonded fiber in an infinite matrix ($1 \times 1 - free$, $V_f = 60\%$). In G_{I0} and G_{II0}, E_2, ν_{12} and ν_{21} are evaluated using the Concentric Cylinders Assembly [28] with Self-Consistent Shear [29] (CCA-SCS) model for $V_f = 60\%$. In both cases, a transverse load is applied in the form of transverse strain ε_x of 1%. *Right*: Mode I and Mode II ERR of single partially debonded fiber in an infinite matrix ($1 \times 1 - free$, $V_f = 60\%$) normalized by Mode I and Mode II ERR of the circular crack in an infinite isotropic medium (G_{I0} and G_{II0}).

tudinal splitting behaviour of glass and carbon fibre reinforced epoxy cross ply laminates and the effect of poisson and thermally generated strain, Proceedings of the Royal Society A: Mathematical, Physical and Engineering Sciences 366 (1727) (1979) 599–623. `doi:10.1098/rspa.1979.0071`.

[7] J. E. Bailey, A. Parvizi, On fibre debonding effects and the mechanism of transverse-ply failure in cross-ply laminates of glass fibre/thermoset composites, Journal of Materials Science 16 (3) (1981) 649–659. `doi:10.1007/bf02402782`.

[8] L. Asp, L. Berglund, R. Talreja, Prediction of matrix-initiated transverse failure in polymer composites, Composites Science and Technology 56 (9) (1996) 1089–1097. `doi:10.1016/0266-3538(96)00074-7`.

[9] J. A. Kies, Maximum strains in the resin of fibreglass composites, Nrl

report 5752, ad-274560, Washington (DC): U.S. Naval Research Laboratory (1962).

[10] H. Zhang, M. Ericson, J. Varna, L. Berglund, Transverse single-fibre test for interfacial debonding in composites: 1. experimental observations, Composites Part A: Applied Science and Manufacturing 28 (4) (1997) 309–315. doi:10.1016/s1359-835x(96)00123-6.

[11] F. París, E. Correa, V. Mantič, Kinking of transversal interface cracks between fiber and matrix, Journal of Applied Mechanics 74 (4) (2007) 703. doi:10.1115/1.2711220.

[12] L. Zhuang, R. Talreja, J. Varna, Transverse crack formation in unidirectional composites by linking of fibre/matrix debond cracks, Composites Part A: Applied Science and Manufacturing 107 (2018) 294–303. doi:10.1016/j.compositesa.2018.01.013.

[13] L. Zhuang, A. Pupurs, J. Varna, R. Talreja, Z. Ayadi, Effects of inter-fiber spacing on fiber-matrix debond crack growth in unidirectional composites under transverse loading, Composites Part A: Applied Science and Manufacturing 109 (2018) 463–471. doi:10.1016/j.compositesa.2018.03.031.

[14] C. Sandino, E. Correa, F. París, Numerical analysis of the influence of a nearby fibre on the interface crack growth in composites under transverse tensile load, Engineering Fracture Mechanics 168 (2016) 58–75. doi:10.1016/j.engfracmech.2016.01.022.

[15] J. Varna, L. Q. Zhuang, A. Pupurs, Z. Ayadi, Growth and interaction of debonds in local clusters of fibers in unidirectional composites during transverse loading, Key Engineering Materials 754 (2017) 63–66. doi:10.4028/www.scientific.net/kem.754.63.

[16] C. Sandino, E. Correa, F. París, Interface crack growth under transverse

compression: nearby fibre effect, in: Proceeding of the 18^{th} European Conference on Composite Materials (ECCM-18), 2018.

[17] M. Comninou, The interface crack, Journal of Applied Mechanics 44 (4) (1977) 631. doi:10.1115/1.3424148.

[18] M. Toya, A crack along the interface of a circular inclusion embedded in an infinite solid, Journal of the Mechanics and Physics of Solids 22 (5) (1974) 325–348. doi:10.1016/0022-5096(74)90002-7.

[19] F. París, J. C. Caño, J. Varna, The fiber-matrix interface crack — a numerical analysis using boundary elements, International Journal of Fracture 82 (1) (1996) 11–29. doi:10.1007/bf00017861.

[20] S. P. Timoshenko, J. N. Goodier, Theory of elasticity, Engineering societies monographs, McGraw-Hill, 1987.

[21] V. Mantič, Interface crack onset at a circular cylindrical inclusion under a remote transverse tension. application of a coupled stress and energy criterion, International Journal of Solids and Structures 46 (6) (2009) 1287–1304. doi:10.1016/j.ijsolstr.2008.10.036.

[22] P. P. Camanho, C. G. Dvila, S. T. Pinho, L. Iannucci, P. Robinson, Prediction of in situ strengths and matrix cracking in composites under transverse tension and in-plane shear, Composites Part A: Applied Science and Manufacturing 37 (2) (2006) 165 – 176, compTest 2004. doi:10.1016/j.compositesa.2005.04.023.

[23] N. Laws, G. Dvorak, M. Hejazi, Stiffness changes in unidirectional composites caused by crack systems, Mechanics of Materials 2 (2) (1983) 123 – 137. doi:10.1016/0167-6636(83)90032-7.

[24] J. Varna, 2.10 crack separation based models for microcracking, in: P. W. Beaumont, C. H. Zweben (Eds.), Comprehensive Composite Materials II, Elsevier, Oxford, 2018, pp. 192 – 220. doi:10.1016/B978-0-12-803581-8.09910-0.

[25] H. Tada, P. Paris, G. Irwin, The Stress Analysis of Cracks Handbook, ASME Press, 2000.

[26] G. I. Barenblatt, Scaling phenomena in fatigue and fracture, International Journal of Fracture 138 (1-4) (2006) 19–35. `doi:10.1007/s10704-006-0036-0`.

[27] N. I. Ioakmidis, P. S. Theocaris, Array of periodic curvilinear cracks in an infinite isotropic medium, Acta Mechanica 28 (1) (1977) 239–254. `doi:10.1007/BF01208801`.

[28] Z. Hashin, Analysis of composite materials—a survey, Journal of Applied Mechanics 50 (3) (1983) 481. `doi:10.1115/1.3167081`.

[29] R. Christensen, K. Lo, Solutions for effective shear properties in three phase sphere and cylinder models, Journal of the Mechanics and Physics of Solids 27 (4) (1979) 315–330. `doi:10.1016/0022-5096(79)90032-2`.

8. Conclusions